A synthesis of the basal thermal state of the Antarctic ice sheet

Owen SEINER[1,2], Anna HUGNEY[1], Hélène SEROUSSI[1], Joseph A. MACGREGOR[3]

[1] *Thayer School of Engineering, Dartmouth College, Hanover, NH, USA*

[2] *Institute for Geophysics, Jackson School of Geosciences, University of Texas at Austin, Austin, TX, USA*

[3] *Cryospheric Sciences Lab, NASA Goddard Space Flight Center, Greenbelt, MD, USA*

Correspondence: <owen.seiner@utexas.edu>

ABSTRACT. The basal thermal state of the Antarctic ice sheet (AIS) – whether the base is frozen or thawed – fundamentally underpins its flow and is an important factor in understanding its large-scale response to external forcings. Here we present a first synthesis of the AIS basal thermal state combining two indirect and independent methods: (1) a compilation of nine three-dimensional thermomechanical simulations that calculate AIS basal temperature as part of the Ice Sheet Model Intercomparison Project for CMIP6 (ISMIP6) and (2) an estimate of the basal slip ratio, defined as the ratio of observed surface speed to deformational speed. This synthesis is evaluated against direct observations from deep boreholes and predicted flowpaths for water originating from subglacial lakes detected by altimetry and radar sounding. The synthesis predicts a thawed bed across most of West Antarctica and localized regions in East Antarctica. Most of the Antarctic Peninsula, the Transantarctic Mountains, and several regions of East Antarctica are likely frozen at the bed. Overall, our synthesis suggests 46% of the AIS bed is likely thawed, 18% likely frozen, and the remaining 36% is uncertain. Additional observations, particularly at continental scale, are required to improve our understanding of Antarctica's basal thermal state.

INTRODUCTION

The basal thermal state of the Antarctic Ice Sheet (AIS), i.e., whether its base is frozen or thawed, is a fundamental control on its flow and response to external forcings (Pattyn, 2010; Dawson and others, 2022, 2024). For example, regions with a thawed base permit significant basal motion (or sliding) at the interface between the ice and bedrock or within any deformable sediment layer directly beneath the ice (Thorsteinsson and Raymond, 2000). Such regions contribute more to sea level rise and are more sensitive to changing climate conditions (Dawson and others, 2022; Levermann and others, 2020; Larter, 2022). A recent study produced the first Antarctic-wide model of subglacial hydrologic conditions, which suggested the widespread presence of subglacial water and highlighted contrasting conditions across the continent: subglacial water thickness varies between 0 and 192 m, with an average of 0.1 m (Ehrenfeucht and others, 2025). In another recent study, Zhao and others (2025) demonstrated the importance of understanding subglacial hydrologic systems and its influence on sliding behavior using an Antarctic ice-sheet model. They found that simulations that incorporated subglacial hydrology increased ice discharge threefold compared to simulations that did not include it, highlighting the importance of the basal thermal state and subglacial hydrology to Antarctic ice dynamics. Additionally, ice-core paleoclimatologists are interested in AIS basal conditions to obtain the oldest possible ice – and thus a longer climatic record – by avoiding drilling where there is significant basal melting (Obase and others, 2023; Van Liefferinge and Pattyn, 2013).

Direct observations of basal thermal conditions are limited to the sites of deep boreholes that reach the ice-sheet base, of which only a handful have been drilled since the 1950s due to their logistical and technical complexity (Ueda, 2007; Talalay, 2023). Beyond these deep boreholes, only indirect methods that rely on a range of observations can be used to estimate the AIS basal thermal state. The basal thermal state is determined by the temperature at the ice base being at or very close to the pressure melting point (thawed ice) or below the pressure melting point (frozen ice). Ideally, the basal temperature would also be constrained, but identification of frozen and thawed regions is a much more tractable problem. The basal thermal state can therefore be reduced to a ternary assessment (frozen, thawed, or uncertain), and the identification of thawed and frozen regions can help constrain basal boundary conditions in models or radar observations, guide site selection for ice-core drilling, or characterize and quantify the potential effects of basal thaw on the AIS at decadal timescales. As a result, conditions at the ice–bed interface are a substantial focus of research, often involving radar observations and numerical modeling (Kang and

others, 2022; Huang and others, 2024; Schroeder and others, 2016).

Conditions at the base of the Greenland Ice Sheet (GrIS) have been investigated by MacGregor and others (2016, hereafter *GBaTSv1*) in 2016 and updated in 2022 MacGregor and others (2022, hereafter *GBaTSv2*). In GBaTSv1, MacGregor and others (2016) combined estimates of GrIS basal conditions derived from eight three-dimensional (3D) thermo-mechanical ice-flow models, one-dimensional (1D) modeling of radiostratigraphy, a comparison of surface velocity with deformational velocity, and Moderate Resolution Imaging Spectro-radiometer (*MODIS*) surface texture. For the GBaTSv2 update, datasets were updated with newer versions and the MODIS surface texture analysis method was discontinued, as Ng and others (2018) demonstrated that surface undulations are not a consistent indicator of a thawed bed. GBaTSv1 and GBaTSv2 provided the first large-scale syntheses of GrIS basal thermal state. Rather than determining pressure-adjusted basal temperature everywhere across the ice-sheet, MacGregor and others (2016) and MacGregor and others (2022) reduce that challenging problem into a ternary classification system, determining a frozen base, a thawed base, or an uncertain region at a 5 km scale across the ice sheet.

Here we present the first synthesis of AIS basal thermal state using a combination of two methods, a compilation of existing 3D thermomechanical AIS simulations and a comparison of observed surface velocity and calculated maximum deformational velocity. The AIS basal thermal synthesis is then evaluated against existing borehole data and inferred basal hydrology from subglacial lakes.

DATA AND METHODS

We first describe the two independent methods used to estimate the AIS basal conditions and the datasets used for each method. We then detail the method and data used for validation, including the process to simulate subglacial hydrologic routing from subglacial lakes and the borehole validation dataset. While the native resolution of the results varies for each method, all the results are re-gridded and synthesized onto the common 8-km grid used for ISMIP6 to simplify direct comparison (Nowicki and others, 2020).

3D thermomechanical modeling of basal thermal temperature

Ice-flow models simulate 3D thermomechanical ice conditions by solving coupled mass-, momentum-, and energy-conservation equations (Larour and others, 2012; Gagliardini and others, 2013; Winkelmann and others, 2011). These models therefore simulate the temperature of the ice at the ice–bed interface beneath

the AIS. The AIS basal thermal state varies between model simulations due to the wide range of initialization methods, model resolution, boundary conditions, external forcings, and choices of model parameters and processes captured in the simulations (Pattyn, 2011; Seroussi and others, 2019, 2024).

Here we use nine ice flow models that took part in ISMIP6-2100 to compile continental-scale basal temperature of the AIS (Nowicki and others, 2020; Seroussi and others, 2020). Using an ensemble of models allows us to capture a range of results and take into account individual model uncertainty by including basal temperature simulated with a wider range of parameterizations, numerical schemes, and initialization procedures. Within the ISMIP6-2100 ensemble, we use the nine models (Table 3) that solve the thermal equation and, therefore, simulate basal ice temperature. The model initialization procedure and length of the historical period varies between models, depending whether they use long spin-ups or assimilate present-day observations (Goelzer and others, 2018; Nowicki and Seroussi, 2018). As we are interested in present-day basal conditions, we select the modeled conditions at the end of the historical period, so conditions used represent modeled conditions by each of the nine models at the beginning of 2015, before the start of future projections. Additionally, for modeling groups that submitted several sets of simulations, we only use one simulation per modeling group, designated as the main contribution by those groups. The basal temperatures calculated from the 3D thermomechanical models are adjusted to capture pressure melting using the modeled ice thickness and assuming a uniform melting-point decrease of $8.7{\cdot}10^{-4}$ K m^{-1} (Cuffey and Paterson, 2010, p. 406). Following MacGregor and others (2022), the transition between frozen and thawed ice is taken to be -1°C, therefore areas with basal temperatures greater than -1°C are presumed to have a thawed base and areas with basal temperatures lower than -1°C are presumed frozen.

Basal slip ratio

The second method estimates areas experiencing basal sliding as a proxy for regions that are likely thawed. Sliding occurs when the ice slides over the underlying bed either through deformation in the basal ice layer or in the underlying sediment layer (Tulaczyk and others, 2000; Cuffey and Paterson, 2010), which requires the ice at the base and the underlying sediments to be at or close to the melting point (Lliboutry, 1987; Echelmeyer and Zhongxiang, 1987; Engelhardt, 2004). We evaluate the ratio between observed surface speed and modeled maximum deformational speed, termed the basal slip ratio, following MacGregor and others (2016). Where the observed surface speed is greater than the column's modeled maximum

deformation speed, the basal slip ratio is greater than unity. Therefore, the observed surface motion cannot be explained by internal deformation only, so basal sliding (and hence a thawed bed) is therefore required to explain observed surface velocities. We use version 2 of the MEaSUREs continental-scale ice surface velocity from Rignot (2017), derived from satellite-based Interferometric Synthetic Aperture Radar (InSAR) data taken across the AIS from 1996 to 2016 and posted on a 450-m resolution grid.

To calculate the maximum possible surface speed due to internal deformation, we use the shallow ice approximation, which captures the large-scale deformation speed (Hutter, 1982; Cuffey and Paterson, 2010) and was used by MacGregor and others (2022). The maximum velocity at the ice surface due to internal deformation is:

$$u_{\mathrm{def}} = \frac{2EH\bar{A}}{n+1}\left(\rho_i g H \alpha\right)^n , \tag{1}$$

where the density of the ice column ρ_i is 917 kg m^{-3}, the rate of acceleration due to gravity g is 9.81 m s^{-2}, the rate factor for ice $\bar{A}$ is temperature-dependent, $E = 2$ is the dimensionless depth-averaged enhancement factor, H is the ice thickness, α is the surface slope, and n is Glen's flow exponent (assumed to be equal to 3). u_{def} is then compared to the observed surface velocity to calculate the basal slip ratio, γ, using the method described in MacGregor and others (2016) as:

$$\gamma = \frac{u_{\mathrm{obs}}}{u_{\mathrm{def}}}. \tag{2}$$

The calculation of the deformational velocity fields from digital elevation models requires smoothing to prevent small-scale features that have horizontal scales at or below the ice thickness from generating spurious results. A spatially varying triangular filter with a width of 10 ice thicknesses is applied to observations of surface velocity and ice thickness. These filtered values are then used to calculate the surface slope. This filter is chosen following recommendations from McCormack and others (2019), who showed that such a filter minimized the residual between calculated and observed surface velocity fields as well as their directions.

As several terms used to calculate the basal slip ratio have potentially large errors, we investigate the sensitivity of the estimated basal thermal state to the choice of rate factor and the uncertainty reported in the thickness and surface-velocity datasets.

We test a range of depth-averaged temperatures, from -18 to 0°C, estimate their corresponding rate factor according to an exponential regression determined using temperature and rate factor values from

Cuffey and Paterson (2010), and recalculate the basal slip ratio and fraction of frozen and thawed base for all these temperatures and rate factors. The rate factor associated with this temperature range is varied linearly, inputted into Equation 1, and then used to calculate the basal slip ratio following Equation 2. For each rate factor (and thus temperature), we calculate the fraction of ice-covered-area assumed to be frozen from the basal slip ratio (Fig. 1).

We find a logistic relationship between the prescribed rate factor and the resulting fraction of frozen bed. Based on these results, we select a value near the inflection point of the standard case to represent our baseline or "standard" estimate; this inflection point is where the frozen fraction is most sensitive to changes in the rate factor and associated temperature. The temperature used for the standard case is -12.7°C. For simplicity, we take the standard temperature associated with the rate factor to be -12°C, which is equivalent to a rate factor of $\bar{A} = 3.22 \cdot 10^{-25}$ Pa s^{-1} (Fig.1).

We also select two additional cases to evaluate the range of plausible basal thermal states, which are equivalent to "cold" and "warm" biased estimates. To capture the effect of uncertainty from the datasets, a maximum and minimum deformation speed are calculated for each grid cell. The uncertainty in ice thickness is added to the ice thickness value (H) in Eq. 1 for the maximum deformation speed case, and subtracted in the minimum deformation speed case. Similarly, a maximum and minimum value is generated for the observed surface velocity based on the uncertainty reported in the MEaSUREs v2 dataset. The warm bias combines the minimum possible observed surface velocity and the maximum deformational velocity, leading to basal conditions that overestimate areas with a basal slip ratio greater than one and therefore may overestimate thawed areas (Table 1). Conversely, the cold bias combines the maximum observed surface velocity and the minimum deformational velocity, leading to basal conditions that overestimate areas with a basal slip ratio less than one. The "cold" and "warm" biased estimates, along with the standard, are also simulated across a range of rate factors and temperatures to reflect their uncertainty in rheology (Fig. 1). For the warm bias case, the selected temperature associated with the rate factor is -18°C, equivalent to $\bar{A} = 1.29 \cdot 10^{-25}$ Pa s^{-1}. For the cold bias case, the chosen temperature associated with the rate factor is -5°C, equivalent to $\bar{A} = 9.34 \cdot 10^{-25}$ Pa s^{-1} (Table 1).

We produce maps of the basal slip ratio for the standard case, the cold bias and the warm bias to evaluate the effect of uncertainties in the ice thickness, surface speed, and rate factor selection.

Table 1. Constants, parameters, and error handling used to calculate the basal slip ratio for the standard case, cold bias, and warm bias.

Constant/Parameter	Standard	Cold Bias	Warm Bias
$\bar{A}$ ($\mathrm{Pa}^{-3}\,\mathrm{s}^{-1}$)	3.22×10^{-25}	9.34×10^{-25}	1.29×10^{-25}
Depth-averaged T (°C)	-12	-5	-18
Thickness (m)	H	$H_{\mathrm{min}} = H - H_{\mathrm{err}}$	$H_{\mathrm{max}} = H + H_{\mathrm{err}}$
Deformational speed, u_{def} ($\mathrm{m} \cdot \mathrm{yr}^{-1}$)	$\frac{2E\,H\,\bar{A}}{n+1}(\rho_{\mathrm{ice}}\,g\,H\,\alpha)^n$	$\frac{2E\,H_{\mathrm{min}}\,\bar{A}}{n+1}(\rho_{\mathrm{ice}}\,g\,H_{\mathrm{min}}\,\alpha)^n$	$\frac{2E\,H_{\mathrm{max}}\,\bar{A}}{n+1}(\rho_{\mathrm{ice}}\,g\,H_{\mathrm{max}}\,\alpha)^n$
Observed speed, u_{obs} ($\mathrm{m} \cdot \mathrm{yr}^{-1}$)	u_{obs}	$u_{\mathrm{obs}} + u_{\mathrm{err}}$	$u_{\mathrm{obs}} - u_{\mathrm{err}}$

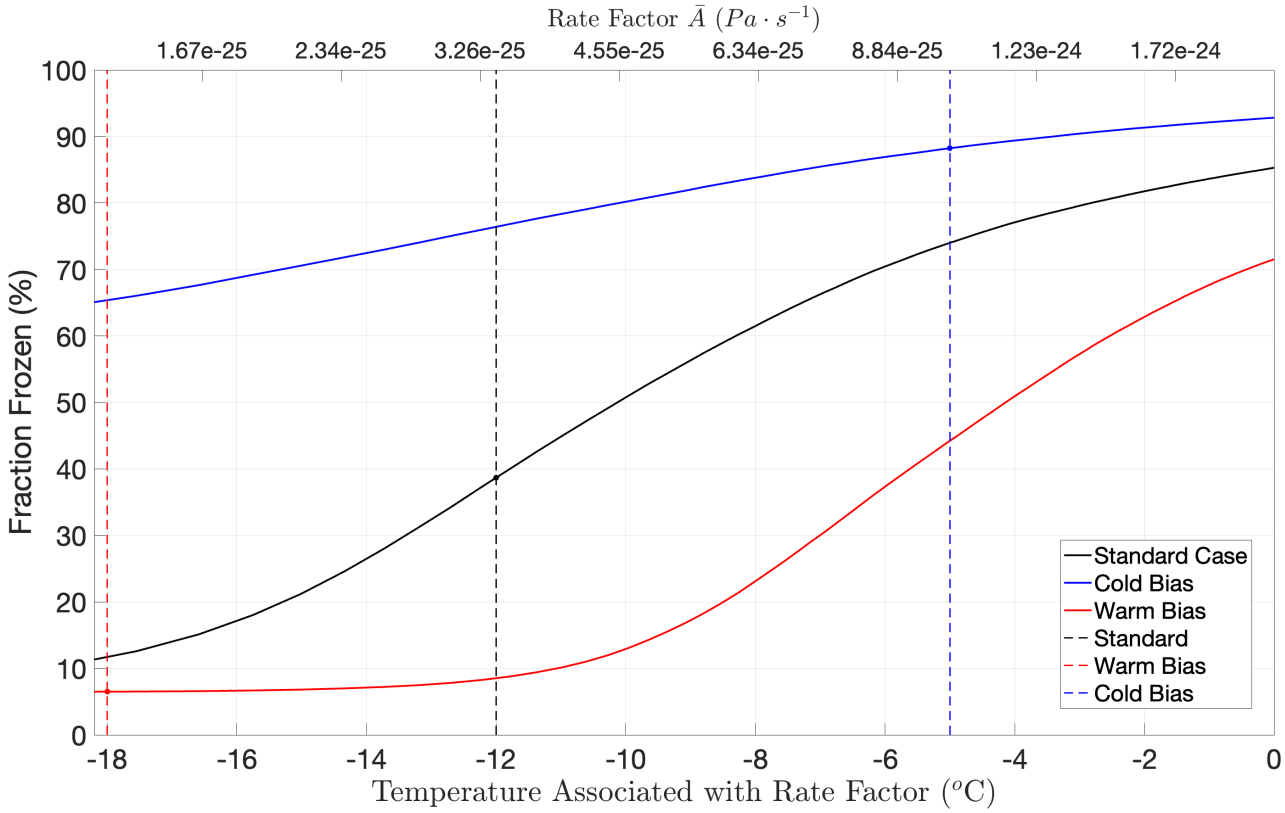

Fig. 1. Fraction of the AIS bed predicted to be frozen by the basal slip ratio method across a range of rate factors (upper x-axis) and associated depth-averaged temperatures (lower x-axis) for: (1) standard, (2) cold bias (minimum), and (3) warm bias (maximum). The vertical dashed line represent the temperatures selected for the standard, cold bias, and warm bias cases.

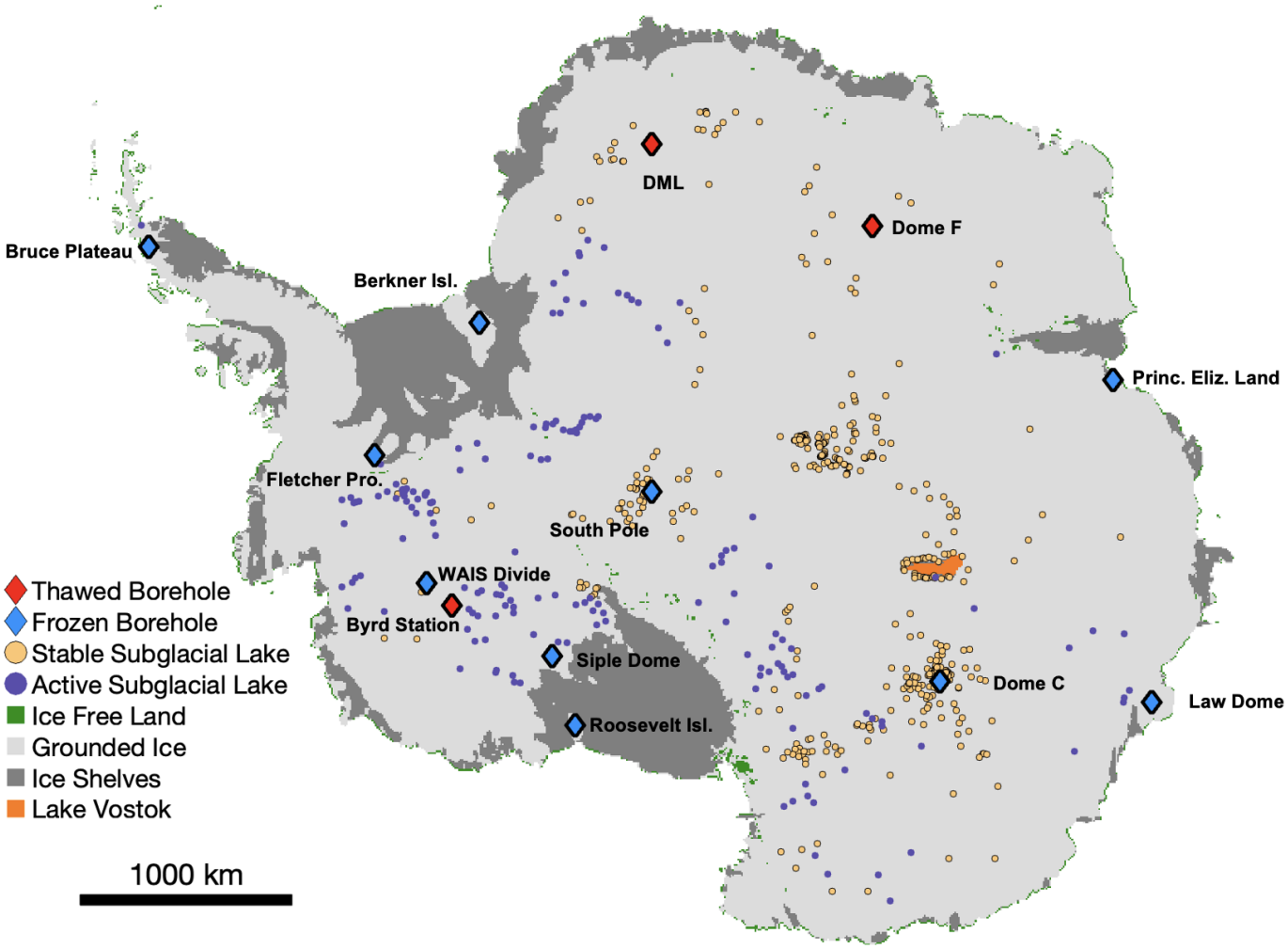

Fig. 2. Antarctic Ice Sheet showing the current extent of grounded ice, ice shelves, and ice-free areas according to BedMachine Antarctica v3 (Morlighem, 2022). Active and stable subglacial lake locations are from Livingstone and others (2022). Borehole locations and basal thermal states at these locations are listed in Table 2. The area of the subglacial lakes and boreholes are inflated relative to their actual size.

Subglacial hydrology

We seek to compare regions estimated to have a thawed bed with the previously identified presence of liquid water at the base of the AIS. Active subglacial lakes are detected from rapid and localized changes in the ice surface elevation detected by altimetry, indicating filling and draining of subglacial lakes (Fricker and others, 2007; Siegfried and others, 2014). Non-active (stable) subglacial lakes are generally identified by radar sounding and are assumed to neither fill or drain rapidly, so that these are closed systems where inflow and outflow are either balanced or small (Wright and Siegert, 2012). Radar identification of stable subglacial lakes comes from bright basal reflections, first observed in the 1960s, and later expanded and fully characterized in the 1990s and 2000s (Siegert and Dowdeswell, 1996; Wolovick and others, 2013). Livingstone and others (2022) recently compiled all subglacial lakes detected so far. Of the 675 subglacial lakes reported for the AIS, more than 80% were detected by radar sounding and are thought to be stable, while the remaining lakes have been observed to fill and drain by surface altimetry and are classified as active (Fig. 2).

We simulate the presence of liquid water at the base of the AIS by initializing subglacial water flow-paths from observed subglacial lakes using a simple routing model based on hydraulic potential. We use TopoToolbox's FLOWobj function and multiple flow direction algorithm (Schwanghart and Scherler, 2014). We perform two versions of these simulations: (1) initialized from active subglacial lakes only; and (2) initialized from all subglacial lakes. We assume that active subglacial lakes contain enough water to generate downstream subglacial channels in all cases, i.e., that water is regularly transported downstream from these active lakes. In the subglacial lake routing using only active lakes, we assume that stable lakes do not discharge downstream and that only the lake itself indicates a locally thawed bed. However, the majority of subglacial lakes are stable and the identification of lakes from altimetry requires measurable surface-elevation change and thus may bias identification of active subglacial lakes toward those with larger discharges. We therefore run a second case where water is assumed to flow from all subglacial lakes, both active and stable.

Subglacial water flow is assumed to follow gradients in subglacial hydraulic potential, which accounts for both subglacial topography and hydrostatic pressure from the overlying ice thickness. This hydraulic potential ϕ is defined as:

$$\phi = \rho_w g z_b + \rho_{ice} g H, \tag{3}$$

Table 2. Direct observations of the basal thermal state from deep Antarctic boreholes. "obs" and "corr" refer to the measured and pressure-corrected basal temperature; "Th" and "Fr" indicate a frozen and thawed assignments, respectively, with no corresponding temperatures.

Site	Lat (°S)	Lon (°E)	Thickness (m)	Temp obs/corr (°C)	Ref.
Bruce Plateau	66.03	–64.07	447	–10.2 / –9.8	Zagorodnov and others (2012)
Byrd Station	80.02	–119.52	2164	Th	Gow and others (1968)
Dome F	75.10	39.70	3035	Th	Motoyama and others (1998)
Law Dome	66.76	112.80	1200	–7.0 / –6.0	Dahl-Jensen and others (1999)
Siple Dome	81.66	–148.81	1005	–2.5 / –1.7	Engelhardt (2004)
South Pole	90.00	0.00	2810	–9.0 / –6.6	Price and others (2002)
WAIS Divide	79.47	–112.09	3405	Fr	Cuffey and Clow (2014)
EPICA Dome C	75.10	–123.40	3286	Fr	Augustin and others (2007)
EPICA DML	75.00	0.00	2774	Th	Wilhelms and others (2014)
Berkner Isl.	79.55	–45.68	948	–11.6 / –10.8	Mulvaney and others (2014)
Fletcher Prom.	77.90	–82.60	654	–18.0 / –17.4	Mulvaney and others (2014)
Roosevelt Isl.	79.36	–161.71	765	–4.3 / –3.6	Fudge and others (2019)
Prin. Eliz. Land	69.59	–76.39	541	–4.5 / –4.1	Talalay and others (2025)

where ρ_i is the ice density (917 kg m^{-3}), ρ_w the density of fresh water (1000 kg m^{-3}), g the acceleration due to gravity (9.81 m s^{-2}), z_b the bed elevation, and H the ice thickness. We use BedMachine Antarctica v3 for the ice thickness and bed topography (Morlighem and others, 2020; Morlighem, 2022). After calculating the hydraulic potential for each point on BedMachine Antarctica's 450-m grid, we use TopoToolbox. These functions use the hydraulic potential gradient to compute water flow accumulation and routing from the lakes towards the Antarctic coast. Water flowpaths are then interpolated onto the 8 km ISMIP6 grid. These flowpaths along with the subglacial lakes are all considered to have a thawed bed and compared to the thawed regions estimated by the 3D thermomechanical model and the basal slip ratio methods.

Borehole validation

The AIS basal thermal synthesis is evaluated against the borehole temperatures measured in thirteen deep Antarctic boreholes (Table 2; Fig. 2). The basal temperature was measured at most sites (Zagorodnov and others, 2012; Dahl-Jensen and others, 1999; Engelhardt, 2004; Price and others, 2002; Mulvaney and others, 2014; Fudge and others, 2019; Talalay and others, 2025), while others only indicate whether the basal ice was frozen or thawed (Gow and others, 1968; Motoyama and others, 1998; Clow and others, 1996; Augustin and others, 2007; Wilhelms and others, 2014; Cuffey and Clow, 2014).

RESULTS

3D thermomechanical modeling of basal temperature

The nine individual 3D thermomechanical models generally show patterns predicting a thawed bed beneath the West Antarctic Ice Sheet (WAIS) and a frozen bed beneath much of the Transantarctic Mountains and the Antarctic Peninsula (Fig. 3). Beneath the East Antarctic Ice Sheet (EAIS), the modeled basal temperatures are both more heterogeneous and differ more substantially between the models. For example, the ILTS-PIK-SICOPOLIS model simulates cold basal temperatures over 77% of the grounded ice, including most of East Antarctica, while the AWI-PISM and PIK-PISM models simulate basal temperatures close to the melting point over 84% and 83% of the AIS, respectively, including most of East Antarctica (Table 3). These differences are caused by different choices made in various model parameters and inputs, including the methods used to initialize them (Goelzer and others, 2018), which remains an active field of research. Another source of uncertainty impacting the basal thermal state of ice sheet models is the geothermal heat flow, which is not well constrained and varies significantly, especially in West Antarctica (Reading and others, 2022; Martos and others, 2017; Stål and others, 2024).

For more than half of the AIS, there is overall a good agreement between the ISMIP6 models: all nine models agree on the basal thermal state for 16% of the total grounded ice area and at least seven of the nine models agree for another 44% of the grounded ice area (Fig. 4). The remaining 40% of the total ice area has less agreement between the nine models. Therefore, significant uncertainty remains for ∼40% of the AIS, based on this assessment of ISMIP6 models. The agreement is overall higher for the WAIS than the EAIS.

We synthesize the results from these numerical models into a binary map showing regions that are likely thawed or frozen (Appendix, Fig. 9). Borehole data confirm the basal state estimated by the models in nine of the thirteen locations. The boreholes that the binary model synthesis predicts incorrectly are WAIS Divide, Dome C, Siple Dome, and Princess Elizabeth Land. These boreholes are located in areas with higher uncertainties that border regions with more consistently thawed or frozen bases, with the exception of Dome C (Fig. 4).

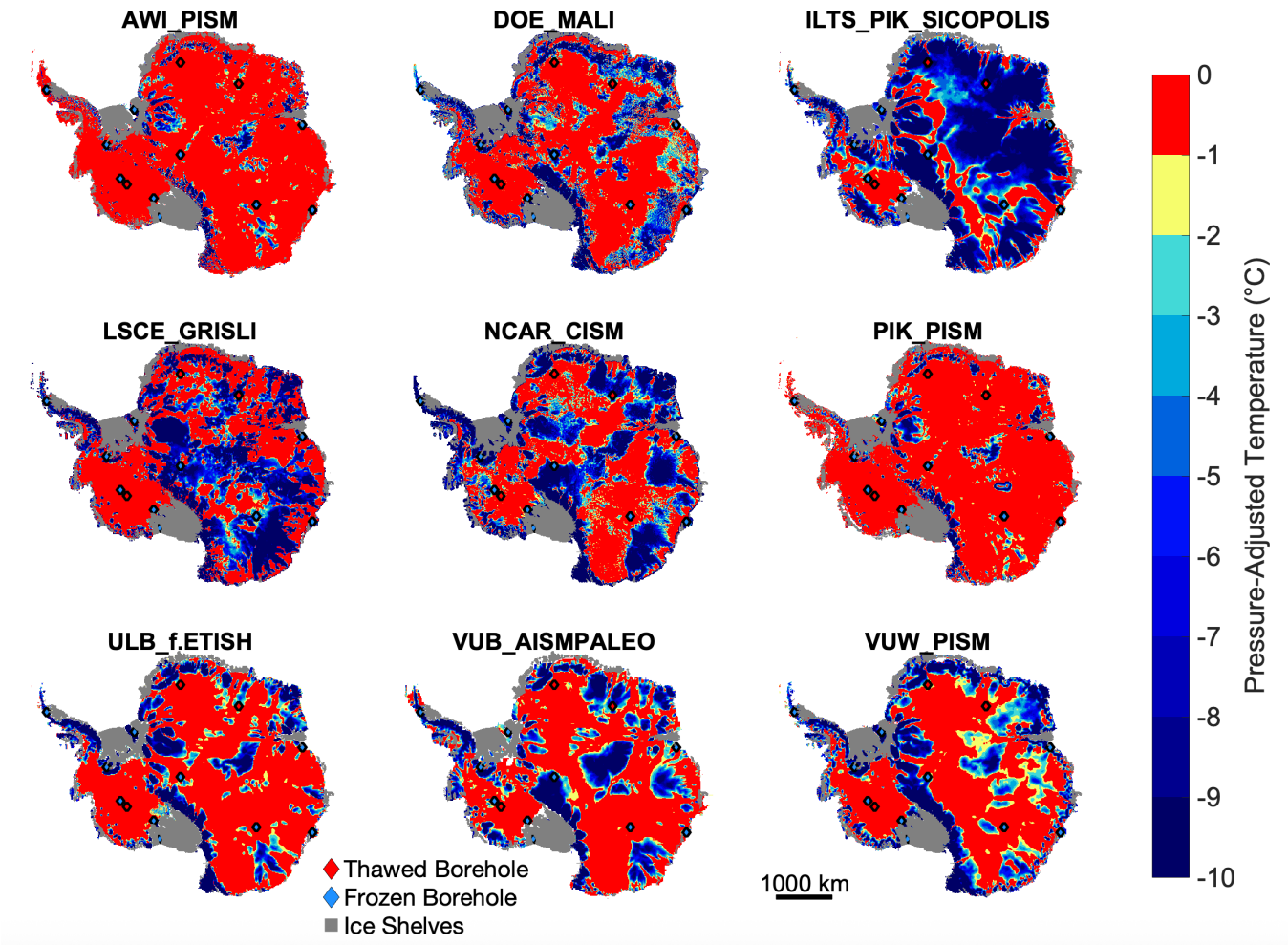

Fig. 3. Pressure-adjusted basal temperature calculated with nine ISMIP6 models. Grey areas represent ice shelf locations and red and blue diamonds indicate deep boreholes with a thawed and frozen bed, respectively.

Table 3. Fraction of grounded basal ice estimated to be frozen and thawed for each ISMIP6 model.

Model	Area frozen (%)	Area thawed (%)
AWI-PISM	16	84
DOE-MALI	45	55
ILTS-PIK-SICOPOLIS	78	22
LCSE-GRISLI	55	45
NCAR-CISM	57	43
PIK-PISM	17	83
ULB-f.ETISH	34	66
VUB-AISMPALEO	43	57
VUW-PISM	47	53

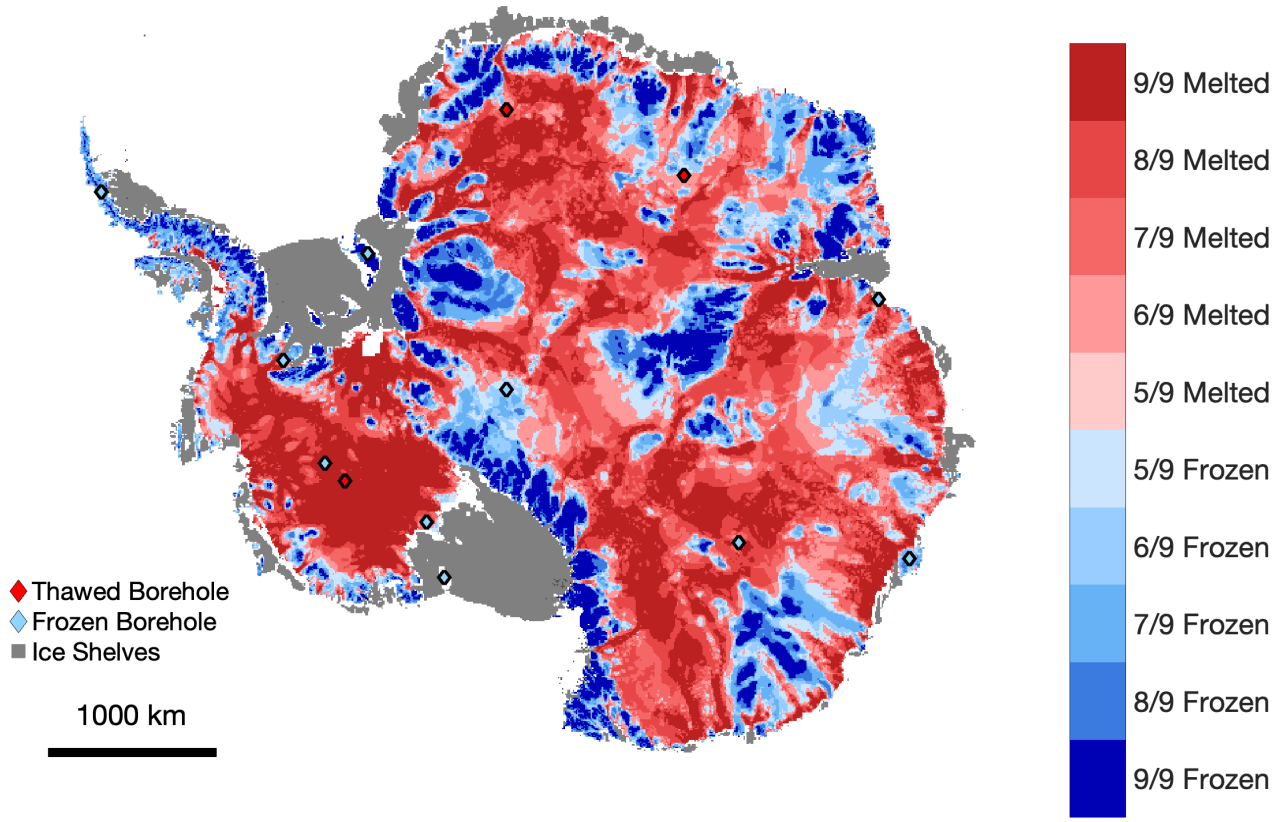

Fig. 4. Agreement between 9 ISMIP6 thermomechanical models shown on Figure 3. Darker colors represent regions where more models agree on the basal thermal state, while lighter colors indicate less agreement. Scattered red and blue diamonds indicate the locations and basal thermal states from deep-drilling boreholes.

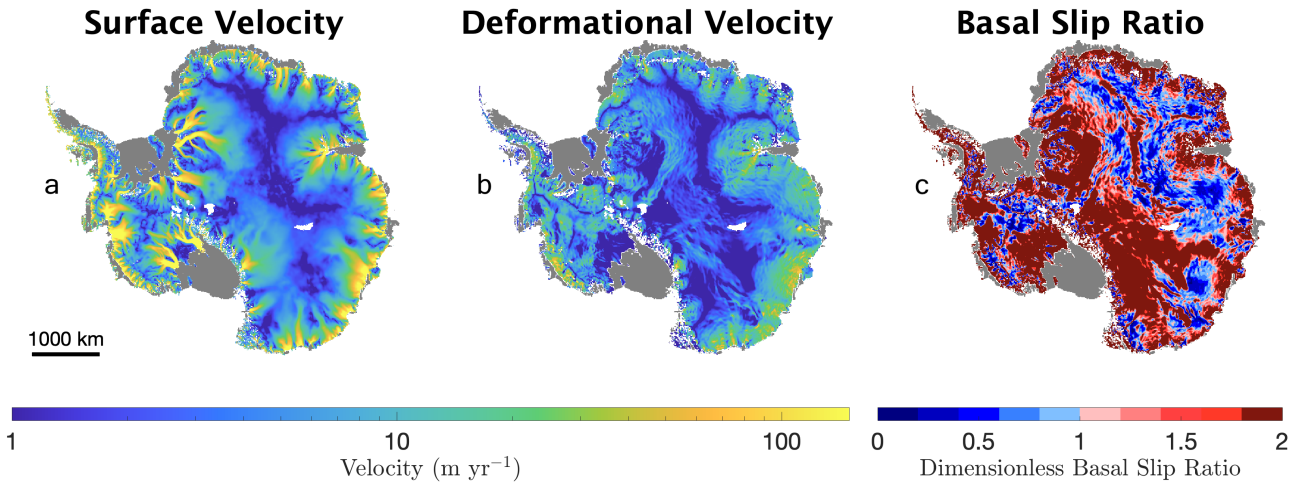

Fig. 5. (a) Observed surface speed of the AIS (Rignot, 2017), (b) standard deformational speed calculated using the Shallow Ice Approximation, and (c) basal slip ratio. Values greater than 1 in the slip ratio indicate basal sliding and thus a locally thawed base.

Basal slip ratio

Observations of surface velocity show fast-flowing ice streams around the continent, with velocities reaching up to about 4000 m yr^{-1} at Thwaites and Pine Island glaciers, and fast velocities propagating hundreds of kilometers upstream from the coast (Fig. 5a). Figure 5b shows the calculated deformational speed over AIS grounded ice for the standard case. Deformational speeds above 150 m yr^{-1} are estimated over large parts of WAIS and in coastal regions of the EAIS, as well as parts of the Antarctic Peninsula. In the ice-sheet interior, deformation speeds are below 10 m yr^{-1} in most places. Figure 5c shows the basal slip ratio, which has values greater than unity across WAIS, particularly in the Thwaites and Pine Island drainage basins, and in the Siple Coast region. Some isolated regions of the Transantarctic Mountains, the Antarctic Peninsula and EAIS also have values greater than unity, while most of the interior EAIS has basal slip ratio below unity.

The basal slip ratio is highly uncertain, primarily due to the selection of values used in the calculation of the deformation of velocity. The rate factor ($\bar{A}$) depends on both the depth-averaged temperature and the enhancement factor (used to adjust for ice softness within the shallow ice approximation), and both are particularly uncertain. The impact of the choices made for the rate factor, ice thickness uncertainty, and surface velocity uncertainty, is highlighted in figure 6. They show the resulting fraction of basal ice predicted to be thawed by the basal slip ratio for the standard, cold bias, and warm bias cases.

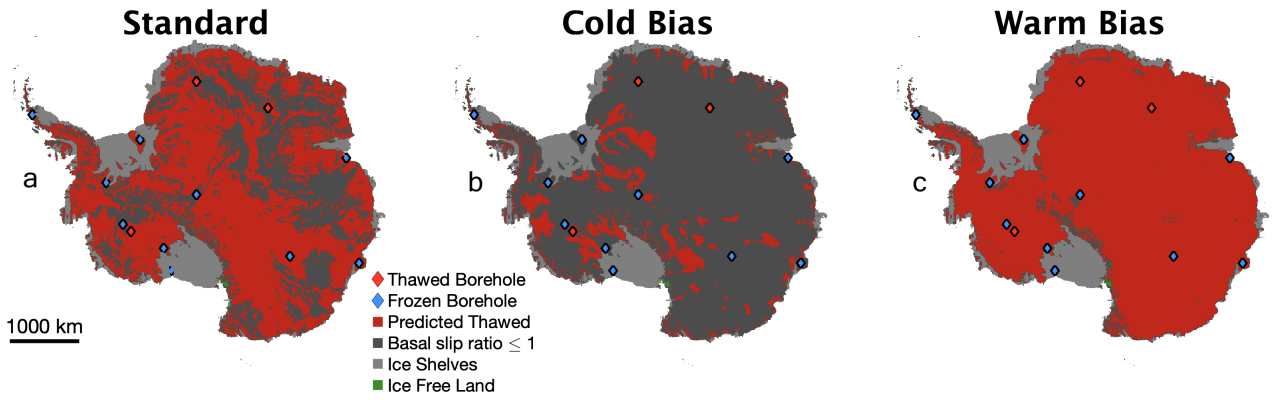

Fig. 6. Thawed areas predicted with the basal slip ratio ($\gamma_{slip} \geqslant 1$) using three different rate factors: (a) standard basal slip ratio, (b) cold biased basal slip ratio, and (c) warm biased basal slip ratio. Data from existing boreholes is added on all three panels with red and blue dots to represent boreholes with a thawed and frozen bed.

The basal slip ratio for the standard case suggests that at least 62% of the grounded ice sheet has a thawed basal thermal state. For these conditions, we find that much of the WAIS and Antarctic Peninsula has a thawed base, while the Transantarctic mountains and heterogeneous regions in EAIS have a frozen base. As the englacial temperature associated with the rate factor warms, the predicted thawed fraction from this method decreases, perhaps counterintuitively. This behavior is the result of the increased rate factor associated with warmer temperatures, leading to an increased deformational velocity, and thus a decreased basal slip ratio. For the cold-biased case, the basal slip ratio, which is generated using a rate factor associated with a warmer depth-averaged temperature of -5°C, the ice deforms more easily and therefore only 12% of the grounded area is predicted to be thawed for Thwaites and Pine Island basins, Siple Coast ice streams, and a few ice streams feeding into Ronne Ice Shelf. In the warm-biased case, the basal slip ratio calculation suggests that 94% of the grounded area is predicted to have a thawed basal thermal state. The results from these extreme cases highlight this method's high sensitivity to the rate factor used to calculate the basal slip ratio, as well as the uncertainty within the observed surface speed and ice-thickness datasets (Fig. 1).

Subglacial hydrology

The subglacial hydrology method estimates the presence of basal water from subglacial lakes and water routing from these lakes. We use it to compare these regions with thawed basal conditions estimated from the 3D models and slip ratio. Figure 2 shows all the subglacial lakes discovered so far (Livingstone and

261 others, 2022) and highlights that active subglacial lakes are predominantly located near the Ross and Ronne
262 Ice Shelves, especially in the Siple Coast, while stable subglacial lakes are predominantly located in the
263 AIS interior. Figure 7a shows subglacial channels originating from all active subglacial lakes, concentrated
264 largely in the WAIS, again predominantly in the Siple Coast, with some additional subglacial channels in
265 the EAIS. Figure 7b shows subglacial channels originating from all subglacial lakes (active and stable), with
266 far more channels extending into the interior of the ice sheet near Dome A and South Pole. The simulated
267 subglacial channels typically connect multiple subglacial lakes within the same subglacial hydrologic basin,
268 as highlighted in previous studies (Fricker and others, 2014). As a result, there is a relatively limited
269 number of subglacial channels simulated.

270 Using active subglacial lakes as seed locations for the routing model, subglacial channels underlay ∼2%
271 of the grounded ice. In the case where we route subglacial water from both active and stable lakes, ∼7%
272 of the grounded ice is inferred to be underlain by water originating from subglacial lakes. Despite good
273 coverage by altimetry and radar sounding, these observations have been recorded only over the past couple
274 decades and can only detect relatively large features. This method therefore captures only a small fraction
275 of the subglacial hydrologic features and underestimates thawed areas, i.e., it has a cold bias as it can
276 only provide indirect evidence of a thawed bed – not a frozen one. Interestingly, the hydrologic routing
277 from subglacial lakes using TopoToolbox's FLOWobj function and multiple flow direction algorithm looks
278 similar overall to the subglacial hydrology generated by Ehrenfeucht and others (2025) using the far more
279 sophisticated Glacier Drainage System Model (GlaDS, Werder and others (2013)) implemented within the
280 Ice-sheet and Sea-level System Model (ISSM v4.24, Larour and others (2012)). The subglacial hydrology
281 results from Ehrenfeucht and others (2025) seem to reflect that the majority hydrologic routing occurs from
282 the active subglacial lakes, but there is likely contribution of some stable subglacial lakes to the overall
283 subglacial hydrology.

284 Synthesis

285 An agreement map combining the results from the two methods as well as the borehole data and the
286 subglacial hydrology was generated on the common 8-km ISMIP6 grid (Appendix, Fig. 9). Areas where
287 the modeling synthesis (Appendix, Fig. 9) and the basal slip ratio (Fig. 6) disagree on the basal thermal
288 state are considered to be uncertain. Results show that most of the WAIS is predicted to be thawed, while
289 the EAIS is generally more heterogeneous, with alternating localized regions of thawed and frozen bed.

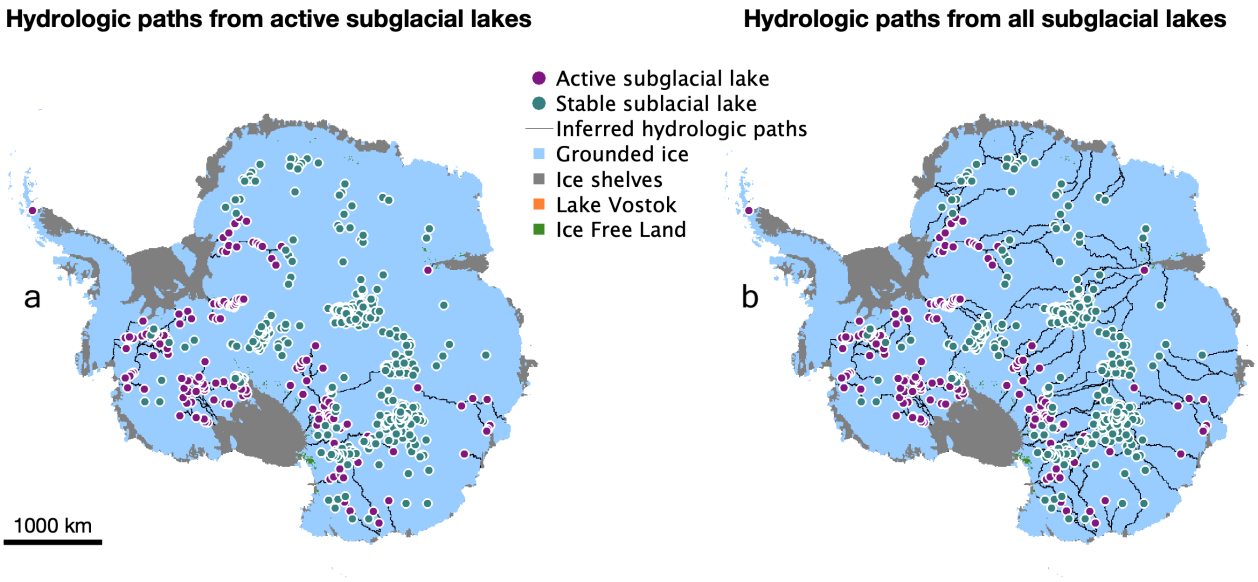

Fig. 7. Subglacial hydrology indicating active subglacial lakes (purple dots), stable subglacial lakes (turquoise dots), and the inferred subglacial streams from both subglacial lakes (black lines). Water originates from active subglacial lakes only (a) and for both active and stable lakes (b). The symbol size of the subglacial lakes is dilated to improve visualization.

Regions with a frozen basal thermal state also include the Transantarctic mountains and the Antarctic Peninsula. Based on the results of the thermomechanical modeling and the basal slip ratio, 18% of the basal thermal state is predicted to be frozen, 46% thawed, and 36% uncertain (Fig. 8 and Table 4). Considered regionally (Table 4), we estimate the WAIS to have the highest fraction of thawed bed and lowest fraction of frozen bed, as compared to the other Antarctic sectors. Almost 40% of the grounded ice area within the WAIS has disagreement between the modeling and basal slip methods. For the EAIS, there is a higher fraction of the grounded ice area expected to be frozen compared to the WAIS, about 19%, while the fraction of uncertain areas is similar to WAIS.

Most boreholes (8 out of 13) fall within areas identified as having an uncertain basal thermal state, and are therefore challenging to use to ground-truth the synthesis between the methods. If we discount the uncertain boreholes from the analysis, 4 out of the 5 boreholes basal thermal states agree with the synthesis. Nine of thirteen borehole data also confirm the basal state estimated overall by the numerical models, as seen in figure 4. In the basal slip method, all 3 thawed boreholes are located in regions with basal slip ratios above unity as seen in figure 6.

The subglacial channels routed from the active lakes (Fig. 8a) almost entirely fall in areas that have

Table 4. Fraction of total grounded ice area predicted to be thawed, frozen, and uncertain, by Antarctic sector.

	Basal thermal state area (%)		
Region	Thawed	Frozen	Uncertain
Whole continent	46	18	36
West Antarctica	53	11	36
East Antarctica	45	19	36
Antarctic Peninsula	8	40	52

a thawed bed, confirming independently that these regions are likely thawed and that these subglacial channels originating from active lakes mostly exist in thawed areas. The results are more nuanced for hydrologic paths originating from both the stable and active lakes (Fig. 8b). Most of the hydrologic paths simulated with the routing algorithm are still located in thawed bed areas, but a few are crossing areas with an uncertain or likely frozen base; this is especially the case in East Antarctica, in the Adélie Land around Dome A.

DISCUSSION AND CONCLUSIONS

We generated a first synthesis of basal thermal state for the AIS based on 3D thermomechanical models and a basal slip ratio that assesses regions likely to experience basal sliding. The synthesis indicates that 46% of the AIS base is likely thawed, 18% likely frozen, and 36% remains too uncertain to characterize. A thawed bed appears widespread in WAIS, but more localized in the interior of EAIS, including east of the Transantarctic Mountains, around the South Pole, and near the grounding zones of the Ross and Ronne ice shelves. Under fast ice streams, there is likely significant subglacial water flux that saturates the sediment and facilitates sliding. The identification of the basal thermal state of the AIS remains uncertain in several areas, with the modeling and basal slip methods disagreeing over about 36% of the grounded ice area.

The areas identified as having a thawed basal thermal state show a similar spatial pattern to regions identified by BedMachine v3 as being grounded below sea level. Of the areas identified by BedMachine v3 to have a bed elevation below sea level, 57% have a thawed basal thermal state, while only 8% of areas identified as being grounded above sea level have a thawed basal thermal state. Of the grid cells predicted to have a thawed basal thermal state, 49% are below sea level and the 51% are above. This implies that, for any location grounded below sea level, there is a much larger chance of that location having a thawed

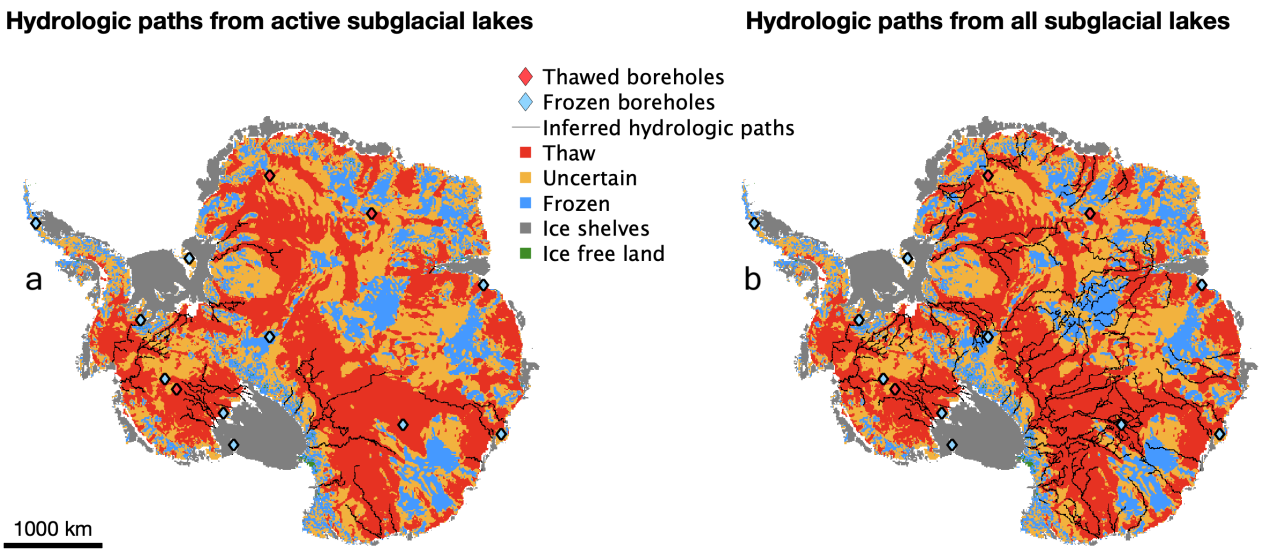

Fig. 8. Agreement map based on the ISMIP6 model results and basal slip ratio methods. Blue indicates that both methods agree on frozen base, red indicates that both methods agree on a thawed base, and yellow indicates regions where the two methods disagree. Observed basal thermal state from deep boreholes are scattered as red (thawed) and blue (frozen) diamonds. Black lines indicate the simulated hydrologic paths from the routing model, with water originating from the active lakes only (a) and from the active and stable lakes (b).

bed than a frozen one.

The substantial remaining uncertainty in our synthesis stems from several factors. One source of uncertainty is the poorly constrained rheology of basal ice, which has distinct chemical and mechanical properties formed by the interaction of ice with basal sediment over long timescales (Hubbard and others, 2009). Fitzsimons and others (2024) also note that sliding has been observed or inferred at temperatures ranging from -1 to -17°C in a variety of glaciers (Cuffey and others, 1999; Echelmeyer and Zhongxiang, 1987; Fitzsimons and others, 2000). Therefore, the basal slip ratio and the synthesis of ISMIP6 models could reasonably disagree if the observation of sliding does not depend only on the basal thermal state, but also on the sediment fraction within the basal ice, as observed by Fitzsimons and others (2024) in shear experiments on basal ice or if a different threshold should be used to separate frozen from thawed conditions. Another source of uncertainty is the challenge of acquiring direct basal temperature data, limiting opportunities for validation of basal temperature models, which produce a range of nominally valid results depending on model inputs and parametrization. Another potential source of uncertainty is the underestimate of areas with frozen basal thermal states. Given the phenomenon of frozen sliding

(Mantelli and Schoof, 2019), the basal slip method may overestimate the presence of basal thaw.

The subglacial hydrology results suggest that most of the uncertain area likely has a frozen basal thermal state (Figs. 7 and 8). In figure 8a, the inferred subglacial hydrology is primarily observed where the basal thermal state is predicted to be frozen, with 85% of active lake originating hydrologic paths overlying predicted thawed regions, 12% overlying uncertain areas and only 3% on in predicted frozen regions. In figure 8b, the inferred subglacial hydrologic channels originating from both active and stable lakes do reach areas classified as having uncertain and frozen basal thermal states. This remains relatively limited as 70% of the inferred hydrologic paths overlap with regions predicted to be thawed, 21% overlaps uncertain regions, and only 9% overlap regions predicted to be frozen (Fig. 8b). Considering these subglacial hydrologic scenarios, the minimal infiltration of subglacial channels into regions predicted to have frozen and uncertain basal thermal states suggests that much of the area classified as uncertain is likely frozen. As discussed in the subglacial hydrology portion of the results, the actual extent of the subglacial hydrologic channels likely lies somewhere between the inferred hydrologic channels in figure 8a and those in figure 8b. However, the assumption that much of the uncertain region likely has a frozen basal thermal state is also complicated by the evidence from the boreholes and comparison with elevation data. While most of the boreholes are located where we identify an uncertain basal thermal state, if we assume the uncertain basal thermal state to be frozen, then only 6 of the 13 borehole basal thermal states are correctly predicted. If we assume the uncertain basal thermal states to be thawed, then 10 of those 13 states are correctly predicted. Therefore, the uncertain region is likely a combination of thawed and frozen basal thermal states, despite the limited intrusion of subglacial hydrologic systems into the uncertain regions.

Beyond the possible sources of uncertainty described above, there is also evidence that the basal thermal conditions vary over short distances and demonstrate spatial heterogeneity in many regions. Dawson and others (2024) used airborne radar sounding observations and binary logistic-regression based classification to determine the basal thermal state beneath the Adelie-George V Coast in East Antarctica. The results show mixed frozen and melted basal thermal states on scales of tens of kilometers, indicating complex basal conditions and the need to estimate the basal thermal state at finer resolution. One promising possibility for improving the basal thermal synthesis of the AIS is the expansion of radar data analysis over the AIS at both higher resolution and continental scale. As demonstrated by Dawson and others (2024) and Schroeder (2022) for the Adelie-George V Coast and the Amundsen Sea Sector, radar data would be an additional and independent indirect method of identifying the basal thermal state due to the temperature dependence

of the englacial attenuation rate and the variance in reflectivity between frozen, thawed, and wet basal thermal conditions.

The results of the basal thermal state synthesis for the AIS differ significantly from the results of the basal thermal syntheses produces for the GrIS, which identified 40% of the GrIS basal thermal state to likely be frozen, 33% thawed, and 28% uncertain (MacGregor and others, 2022). The pattern of GrIS thawed bed is also more structured than that of the AIS, with a frozen interior, melting along the coast and under fast-flowing ice streams, while uncertain regions are largely localized within the transition zones between these areas. Compared with GBaTSv2, the predicted basal thermal state of the AIS has a higher percentage of expected thaw, a lower fraction of likely frozen bed, and higher uncertainty. Antarctica experiences colder surface temperatures than Greenland but has thicker ice than Greenland overall, decreasing the pressure melting point in large regions inland and facilitating melting in interior regions, along with generally higher geothermal heat flow, particularly beneath the WAIS. These competing processes create a more heterogeneous basal thermal state synthesis for the AIS, with a complex combination of thawed and frozen bases, especially in EAIS. The ice is melting not only under fast flowing ice streams but also in almost stagnant but very thick areas, where the very thick ice decreases the pressure melting point by several degrees.

The uncertainty in predicting the basal thermal state of the AIS comes from the limited knowledge of geothermal heat flow below the ice sheet, the high variability within basal thermal state at small spatial scales, the need for denser radar tracks and longer records of surface altimetry. Improvements in our understanding of the AIS basal thermal state require additional data, particularly in the form of additional borehole temperature profiles, analysis of radiostratigraphy and collection and analysis of radar bed reflectivities. Increasing the coverage and analysis of existing results (e.g., Schroeder and al., 2017) would open new opportunities to refine our understanding of Antarctic basal conditions.

OPEN RESEARCH

The BedMachine and MEaSUREs datasets are accessible on the National Snow and Ice Data Center (NSIDC) website. The ISMIP6 data is accessible on GHub:
`https://theghub.org/resources?id=4745`.
Code used to generate basal syntheses and individual figures can be found on:
`https://github.com/owenseiner/AIS_BaTh_v1`

Results from the modeling and basal slip methods, subglacial hydrology mapping, and synthesis generation, can be found on: Zenodo (doi: 10.5281/zenodo.15556691)

ACKNOWLEDGEMENTS

Helene Seroussi was supported by a grant from the Novo Nordisk Foundation under the Challenge Programme 2023 - Grant number NNF23OC00807040. Owen Seiner and Anna Hugney were supported by Undergraduate Research Assistantships at Dartmouth (URAD). Joseph MacGregor acknowledges support from the NASA Cryospheric Sciences Internal Scientist Funding Model (ISFM).

REFERENCES

Augustin L, Panichi S and Frascati F (2007) Epica Dome C 2 drilling operations: performances, difficulties, results. *Annals of Glaciology*, **47**, 68–72 (doi: 10.3189/172756407786857767)

Clow GD, Saltus RW and Waddington ED (1996) A new high-precision borehole-temperature logging system used at GISP2, Greenland, and Taylor Dome, Antarctica. *Journal of Glaciology*, **42**(142), 576–584 (doi: 10.3189/S0022143000003555)

Cuffey KM and Clow GD (2014) Temperature profile of the West Antarctic ice sheet divide deep borehole. *U.S. Antarctic Program (USAP) Data Center* (doi: 10.7265/N5V69GJW)

Cuffey KM and Paterson WSB (2010) *The physics of glaciers*. Elsevier, Oxford, 4th edition

Cuffey KM, Conway H, Hallet B, Gades AM and Raymond CF (1999) Interfacial water in polar glaciers and glacier sliding at -17°C. *Geophysical Research Letters*, **26**(6), 751–754 (doi: 10.1029/1999GL900096)

Dahl-Jensen D, Morgan VI and Elcheikh A (1999) Monte Carlo inverse modelling of the Law Dome (Antarctica) temperature profile. *Annals of Glaciology*, **29**, 145–150 (doi: 10.3189/172756499781821102)

Dawson EJ, Schroeder DM, Chu W, Mantelli E and Seroussi H (2022) Ice mass loss sensitivity to the Antarctic ice sheet basal thermal state. *Nature Communications*, **13**(4957) (doi: 10.1038/s41467-022-32632-2)

Dawson EJ, Schroeder DM, Chu W, Mantelli E and Seroussi H (2024) Heterogeneous basal thermal conditions underpinning the Adélie-George V Coast, East Antarctica. *Geophysical Research Letters*, **51**(2), e2023GL105450 (doi: 10.1029/2023GL105450)

Echelmeyer K and Zhongxiang W (1987) Direct Observation of Basal Sliding and Deformation of Basal Drift at Sub-Freezing Temperatures. *Journal of Glaciology*, **33**(113), 83–98 (doi: 10.3189/S0022143000005396)

Ehrenfeucht S, Dow C, McArthur K, Morlighem M and McCormack FS (2025) Antarctic wide subglacial hydrology modeling. *Geophysical Research Letters*, **52**(1), e2024GL111386 (doi: 10.1029/2024GL111386)

Engelhardt H (2004) Thermal regime and dynamics of the West Antarctic ice sheet. *Annals of Glaciology*, **39**, 85–92 (doi: 10.3189/172756404781814203)

Fitzsimons S, Samyn D and Lorrain R (2024) Deformation, Strength and Tectonic Evolution of Basal Ice in Taylor Glacier, Antarctica. *Journal of Geophysical Research: Earth Surface*, **129**(4), e2023JF007456 (doi: 10.1029/2023JF007456)

Fitzsimons SJ, Lorrain RD and Vandergoes MJ (2000) Behaviour of subglacial sediment and basal ice in a cold glacier. *Geological Society, London, Special Publications*, **176**(1), 181–190 (doi: 10.1144/GSL.SP.2000.176.01.14)

Fricker HA, Scambos T, Bindschadler R and Padman L (2007) An Active Subglacial Water System in West Antarctica Mapped from Space. *Science*, **315**, 1544–1548 (doi: 10.1126/science.1136897)

Fricker HA, Carter SP, Bell RE and Scambos T (2014) Active lakes of Recovery Ice Stream, East Antarctica: a bedrock-controlled subglacial hydrological system. *Journal of Glaciology*, **60**(223), 1015–1030 (doi: 10.3189/2014JoG14J063)

Fudge TJ, Biyani SC, Clemens-Sewall D and Hawley RL (2019) Constraining geothermal flux at coastal domes of the Ross ice sheet, Antarctica. *Geophysical Research Letters*, **46**(22), 13090–13098 (doi: 10.1029/2019GL084332)

Gagliardini O, Zwinger T, Gillet-Chaulet F, Durand G, Favier L, de Fleurian B, Greve R, Malinen M, Martín C, Råback P, Ruokolainen J, Sacchettini M, Schäfer M, Seddik H and Thies J (2013) Capabilities and performance of Emer/Ice, a new-generation ice sheet model. *Geoscientific Model Development*, **6**(4), 1299–1318 (doi: 10.5194/gmd-6-1299-2013)

Goelzer H, Nowicki S, Edwards T, Beckley M, Abe-Ouchi A, Aschwanden A, Calov R, Gagliardini O, Gillet-Chaulet F, Golledge NR, Gregory J, Greve R, Humbert A, Huybrechts P, Kennedy JH, Larour E, Lipscomb WH, Leclec'h S, Lee V, Morlighem M, Pattyn F, Payne AJ, Rodehacke C, Rückamp M, Saito F, Schlegel N, Seroussi H, Shepherd A, Sun S, van de Wal R and Ziemen FA (2018) Design and results of the ice sheet model initialisation experiments initMIP-Greenland: an ISMIP6 intercomparison. *The Cryosphere*, **12**(4), 1433–1460 (doi: 10.5194/tc-12-1433-2018)

Gow AJ, Ueda HT and Garfield DE (1968) Antarctic Ice Sheet: Preliminary Results of First Core Hole to Bedrock. *Science*, **161**(3845), 1011–1013 (doi: 10.1126/science.161.3845.1011)

Huang Y, Zhao L, Wolovick M, Ma Y and Moore JC (2024) Using specularity content to evaluate eight geothermal heat flow maps of Totten Glacier. *The Cryosphere*, **18**(1), 103–119 (doi: 10.5194/tc-18-103-2024)

Hubbard B, Cook S and Coulson H (2009) Basal ice facies: a review and unifying approach. *Quaternary Science Reviews*, **28**(19), 1956–1969 (doi: 10.1016/j.quascirev.2009.03.005)

Hutter K (1982) Dynamics of glaciers and large ice masses. *Annual Review of Fluid Mechanics*, **14**, 87–130 (doi: 10.1146/annurev.fl.14.010182.000511)

Kang H, Zhao L, Wolovick M and Moore JC (2022) Evaluation of six geothermal heat flux maps for the Antarctic Lambert–Amery glacial system. *The Cryosphere*, **16**(9), 3619–3633 (doi: 10.5194/tc-16-3619-2022)

Larour E, Seroussi H, Morlighem M and Rignot E (2012) Continental scale, high order, high spatial resolution, ice sheet modeling using the Ice Sheet System Model (ISSM). *Journal of Geophysical Research*, **117**(F1), F01022 (doi: 10.1029/2011JF002140)

Larter RD (2022) Basal Melting, Roughness and Structural Integrity of Ice Shelves. *Geophysical Research Letters*, **49**(4), e2021GL097421 (doi: 10.1029/2021GL097421)

Levermann A, Winkelmann R, Albrecht T, Goelzer H, Golledge NR, Greve R, Huybrechts P, Jordan J, Leguy G, Martin D, Morlighem M, Pattyn F, Pollard D, Quiquet A, Rodehacke C, Seroussi H, Sutter J, Zhang T, Van Breedam J, DeConto R, Dumas C, Garbe J, Gudmundsson GH, Hoffman MJ, Humbert A, Kleiner T, Lipscomb W, Meinshausen M, Ng E, Perego M, Price SF, Saito F, Schlegel NJ, Sun S and van de Wal RSW (2020) Projecting Antarctica's contribution to future sea level rise from basal ice-shelf melt using linear response functions of 16 ice sheet models (LARMIP-2). *Earth System Dynamics*, **11**(1), 35–76 (doi: 10.5194/esd-11-35-2020)

Livingstone S, Li Y, Rutishauser R, Sanderson R, Winter K, Mikucki J, Björnsson H, Bowling J, Chu W, Dow CF, Fricker HA, McMillan M, FSL N, Ross N, Siegert M, Siegfried M and Sole A (2022) Subglacial lakes and their changing role in a warming climate. *Nature Reviews Earth & Environment*, **3**(4957), 106–124 (doi: 10.1038/s43017-021-00246-9)

Lliboutry L (1987) Realistic yet simple bottom boundary condition for glaciers and ice sheet. *Journal of Geophysical Research*, **92**(B9), 9101–9109 (doi: 10.1029/JB092iB09p09101)

MacGregor JA, Fahnestock MA, Catania GA, Aschwanden A, Clow GD, Colgan WT, Gogineni SP, Morlighem M, Nowicki SMJ, Paden JD, Price SF and Seroussi H (2016) A synthesis of the basal thermal state of the Greenland Ice Sheet. *Journal of Geophysical Research*, **121**(7), 1328–1350 (doi: 10.1002/2015JF003803), 2015JF003803

MacGregor JA, Chu W, Colgan WT, Fahnestock MA, Felikson D, Karlsson NB, Nowicki SMJ and Studinger M (2022) GBaTSv2: a revised synthesis of the likely basal thermal state of the Greenland Ice Sheet. *The Cryosphere*, **16**, 3033–3049 (doi: 10.5194/tc-16-3033-2022)

Mantelli E and Schoof C (2019) Ice sheet flow with thermally activated sliding. Part 2: the stability of subtemperate regions. *Proceedings of the Royal Society A: Mathematical, Physical and Engineering Sciences*, **475** (doi: 10.1098/rspa.2019.0411)

Martos YM, Catalán M, Jordan TA, Golynsky A, Golynsky D, Eagles G and Vaughan DG (2017) Heat flux distribution of Antarctica unveiled. *Geophysical Research Letters*, **44**, 11417–11426 (doi: 10.1002/2017GL075609)

McCormack FS, Roberts JL, Jong LM, Young DA and Beem LH (2019) A note on digital elevation model smoothing and driving stresses. *Polar Research*, **38**(3498) (doi: 10.33265/polar.v38.3498)

Morlighem M (2022) MEaSUREs BedMachine Antarctica, Version 3. *NASA National Snow and Ice Data Center Distributed Active Archive Center* (doi: 10.5067/FPSU0V1MWUB6)

Morlighem M, Rignot E, Binder T, Blankenship D, Drews R, Eagles G, Eisen O, Ferraccioli F, Forsberg R, Fretwell P, Goel V, Greenbaum JS, Gudmundsson H, Guo J, Helm V, Hofstede C, Howat I, Humbert A, Jokat W, Karlsson NB, Lee WS, Matsuoka K, Millan R, Mouginot J, Paden J, Pattyn F, Roberts J, Rosier S, Ruppel A, Seroussi H, Smith EC, Steinhage D, Sun B, Broeke MRvd, Ommen TDv, Wessem Mv and Young DA (2020) Deep glacial troughs and stabilizing ridges unveiled beneath the margins of the Antarctic ice sheet. *Nature Geoscience*, **13**(2), 132–137 (doi: 10.1038/s41561-019-0510-8)

Motoyama H, Takahashi A, Tanaka Y, Shinbori K, Miyahara M, Yoshimoto T, Fujii Y, Furusaki A, Azuma N, Ozawa Y, Kobayashi A and Yoshise Y (1998) Deep ice-core drilling at Dome Fuji and glaciological studies in east Dronning Maud Land, Antarctica. *Annals of Glaciology*, **27**, 333–337 (doi: 10.3189/1998AoG27-1-333-337)

Mulvaney R, Triest J and Alemany O (2014) The James Ross Island and the Fletcher Promontory ice-core drilling projects. *Annals of Glaciology*, **55**(68), 179–188 (doi: 10.3189/2014AoG68A044)

Ng F, Igneczil A, Sole A and Livinston S (2018) Response of Surface Topography to Basal Variability Along Glacial Flowlines. *Journal of Geophysical Research*, **123**(10), 2319–2340 (doi: 10.1029/2017JF004555)

Nowicki S and Seroussi H (2018) Projections of future sea level contributions from the Greenland and Antarctic Ice Sheets: Challenges beyond dynamical ice sheet modeling. *Oceanography*, **31**(2), 109–117 (doi: 10.5670/oceanog.2018.216)

Nowicki S, Goelzer H, Seroussi H, Payne AJ, Lipscomb WH, Abe-Ouchi A, Agosta C, Alexander P, Asay-Davis XS, Barthel A, Bracegirdle TJ, Cullather R, Felikson D, Fettweis X, Gregory JM, Hattermann T, Jourdain NC, Kuipers Munneke P, Larour E, Little CM, Morlighem M, Nias I, Shepherd A, Simon E, Slater D, Smith RS, Straneo F, Trusel LD, van den Broeke MR and van de Wal R (2020) Experimental protocol for sea level projections from ISMIP6 stand-alone ice sheet models. *The Cryosphere*, **14**(7), 2331–2368 (doi: 10.5194/tc-14-2331-2020)

Obase T, Abe-Ouchi A, Saito F, Tsutaki S, Fujita S, Kawamura K and Motoyama H (2023) A one-dimensional temperature and age modeling study for selecting the drill site of the oldest ice core near Dome Fuji, Antarctica. *The Cryosphere*, **17**(6), 2543–2562 (doi: 10.5194/tc-17-2543-2023)

Pattyn F (2010) Antarctic subglacial conditions inferred from a hybrid ice sheet/ice stream model. *Earth and Planetary Science Letters*, **295**, 451–461 (doi: 10.1016/j.epsl.2010.04.025)

Pattyn F (2011) Antarctic subglacial lake discharges. *Antarctic Subglacial Aquatic Environments*, **3**, 27–44 (doi: 10.1029/2010gm000935)

Price PB, Nagornov OV, Bay R, Chirkin D, He Y, Miocinovic P, Richards A, Woschnagg K, Koci B and Zagorodnov V (2002) Temperature profile for glacial ice at the South Pole: Implications for life in a nearby subglacial lake. *Proceedings of the National Academy of Sciences: Earth, Atmospheric and Planetary Sciences*, **99**(12), 7844–7847 (doi: 10.1073/pnas.082238999)

Reading A, Stal T, Halpin J, Losing M, Ebbing J, Shen W, McCormack FS, Siddoway CS and Hasterok D (2022) Antarctic geothermal heat flow and its implications for tectonics and ice sheets. *Nature Reviews Earth & Environment*, **3**, 814–831 (doi: 10.1038/s43017-022-00348-y)

Rignot E (2017) MEaSUREs InSAR-based Antarctica ice velocity map, version 2. *National Snow Ice Data Center* (doi: 10.5067/D7GK8F5J8M8R)

Schroeder DM (2022) Paths forward in radioglaciology. *Annals of Glaciology*, **63**(87-89), 13–17 (doi: 10.1017/aog.2023.3)

Schroeder DM, Seroussi H, Chu W and Young DA (2016) Adaptively constraining radar attenuation and temperature across the Thwaites Glacier catchment using bed echoes. *Journal of Glaciology*, **62**(236), 1075–1082 (doi: 10.1017/jog.2016.100)

Schroeder L and al (2017) Validation of satellite altimetry by kinematic GNSS in central East Antarctica. *The Cryosphere*, 1–28 (doi: 10.5194/tc-11-1111-2017)

Schwanghart W and Scherler D (2014) TopoToolbox 2 – MATLAB-based software for topographic analysis and modeling in Earth surface sciences. *Earth Surface Dynamics*, **2**, 1–7 (doi: 10.5194/esurf-2-1-2014)

Seroussi H, Nowicki S, Simon E, Abe-Ouchi A, Albrecht T, Brondex J, Cornford S, Dumas C, Gillet-Chaulet F, Goelzer H, Golledge NR, Gregory JM, Greve R, Hoffman MJ, Humbert A, Huybrechts P, Kleiner T, Larour E, Leguy G, Lipscomb WH, Lowry D, Mengel M, Morlighem M, Pattyn F, Payne AJ, Pollard D, Price SF, Quiquet A, Reerink TJ, Reese R, Rodehacke CB, Schlegel NJ, Shepherd A, Sun S, Sutter J, Van Breedam J, van de Wal

RSW, Winkelmann R and Zhang T (2019) initMIP-Antarctica: an ice sheet model initialization experiment of ISMIP6. *The Cryosphere*, **13**(5), 1441–1471 (doi: 10.5194/tc-13-1441-2019)

Seroussi H, Nowicki S, Payne AJ, Goelzer H, Lipscomb WH, Abe-Ouchi A, Agosta C, Albrecht T, Asay-Davis X, Barthel A, Calov R, Cullather R, Dumas C, Galton-Fenzi BK, Gladstone R, Golledge NR, Gregory JM, Greve R, Hattermann T, Hoffman MJ, Humbert A, Huybrechts P, Jourdain NC, Kleiner T, Larour E, Leguy GR, Lowry DP, Little CM, Morlighem M, Pattyn F, Pelle T, Price SF, Quiquet A, Reese R, Schlegel NJ, Shepherd A, Simon E, Smith RS, Straneo F, Sun S, Trusel LD, Van Breedam J, van de Wal RSW, Winkelmann R, Zhao C, Zhang T and Zwinger T (2020) ISMIP6 Antarctica: a multi-model ensemble of the Antarctic ice sheet evolution over the 21st century. *The Cryosphere*, **14**, 3033–3070 (doi: 10.5194/tc-14-3033-2020)

Seroussi H, Pelle T, Lipscomb WH, Abe-Ouchi A, Albrecht T, Alvarez-Solas J, Asay-Davis X, Barre JB, Berends CJ, Bernales J, Blasco J, Caillet J, Chandler DM, Coulon V, Cullather R, Dumas C, Galton-Fenzi BK, Garbe J, Gillet-Chaulet F, Gladstone R, Goelzer H, Golledge N, Greve R, Gudmundsson GH, Han HK, Hillebrand TR, Hoffman MJ, Huybrechts P, Jourdain NC, Klose AK, Langebroek PM, Leguy GR, Lowry DP, Mathiot P, Montoya M, Morlighem M, Nowicki S, Pattyn F, Payne AJ, Quiquet A, Reese R, Robinson A, Saraste L, Simon EG, Sun S, Twarog JP, Trusel LD, Urruty B, Van Breedam J, van de Wal RSW, Wang Y, Zhao C and Zwinger T (2024) Evolution of the antarctic ice sheet over the next three centuries from an ismip6 model ensemble. *Earth's Future*, **12**(9), e2024EF004561 (doi: 10.1029/2024EF004561)

Siegert MJ and Dowdeswell JA (1996) Spatial variations in heat at the base of the Antarctic ice sheet from analysis of the thermal regime above subglacial lakes. *Journal of Glaciology*, **42**(142), 501–509 (doi: 10.3189/S0022143000003488)

Siegfried MR, Fricker HA, Roberts M, Scambos TA and Tulaczyk S (2014) A decade of West Antarctic subglacial lake interactions from combined ICESat and CryoSat-2 altimetry. *Geophysical Research Letters*, **41**(3) (doi: 10.1002/2013GL058616)

Stål T, Halpin JA, Goodge JW and Reading AM (2024) Geology Matters for Antarctic Geothermal Heat. *Geophysical Research Letters*, **51**(13), e2024GL110098 (doi: 10.1029/2024GL110098)

Talalay PG (2023) Deep drilling in Antarctic ice: Methods and perspectives. *Earth Science Reviews*, **243**, 104471 (doi: 10.1016/j.earscirev.2023.104471)

Talalay PG, Leitchenkov G, Lipenkov V, Sun Y, Zhang N, Gong D, Liu Y, Li Y, Sun Y, Abdrakhmanov I, Vorobyev M, Khalimov D, Fan X, Salamatin A, Ekaykin AA and Li B (2025) Rare ice-base temperature measurements in Antarctica reveal a cold base in contrast with predictions. *Nature Communications Earth & Environment*, **6**(1), 189 (doi: 10.1038/s43247-025-02127-1)

Thorsteinsson T and Raymond CF (2000) Sliding versus till deformation in the fast motion of an ice stream over a viscous till. *Journal of Glaciology*, **46**(155), 633–640 (doi: 10.3189/172756500781832729)

Tulaczyk S, Kamb WB and Engelhardt HF (2000) Basal mechanics of Ice Stream B, West Antarctica: 1. Till mechanics. *Journal of Geophysical Research: Solid Earth*, **105**(B1), 463–481 (doi: 10.1029/1999JB900329)

Ueda HT (2007) Byrd station drilling 1966–69. *Annals of Glaciology*, **47**, 24–27 (doi: 10.3189/172756407786857631)

Van Liefferinge B and Pattyn F (2013) Using ice-flow models to evaluate potential sites of million year-old ice in Antarctica. *Climate of the Past*, **9**(5), 2335–2345 (doi: 10.5194/cp-9-2335-2013)

Werder MA, Hewitt IJ, Schoof CG and Flowers GE (2013) Modeling channelized and distributed subglacial drainage in two dimensions. *Journal of Geophysical Research*, **118**, 1–19 (doi: 10.1002/jgrf.20146,)

Wilhelms F, Miller H, Gerasimoff MD, Drücker C, Frenzel A, Fritzsche D, Grobe H, Hansen SB, Hilmarsson SA, Hoffmann G and et al (2014) The EPICA Dronning Maud Land deep drilling operation. *Annals of Glaciology*, **55**(68), 355–366 (doi: 10.3189/2014AoG68A189)

Winkelmann R, Martin MA, Haseloff M, Albrecht T, Bueler E, Khroulev C and Levermann A (2011) The Potsdam Parallel Ice Sheet Model (PISM-PIK) - Part 1: Model description. *The Cryosphere*, **5**(3), 715–726 (doi: 10.5194/tc-5-715-2011)

Wolovick MJ, Bell RE, Creyts TT and Frearson NP (2013) Identification and control of subglacial water networks under Dome A, Antarctica. *Journal of Geophysical Research*, **118**(1), 140–154 (doi: 10.7916/D8F769JN)

Wright A and Siegert M (2012) A fourth inventory of Antarctic subglacial lakes. *Antarctic Science*, **24**(6), 659–664 (doi: 10.1017/S095410201200048X)

Zagorodnov V, Nagornov O, Scambos TA, Muto A, Mosley-Thompson E, Pettit EC and Tyuflin S (2012) Borehole temperatures reveal details of 20th century warming at Bruce Plateau, Antarctic Peninsula. *The Cryosphere*, **6**(3), 675–686 (doi: 10.5194/tc-6-675-2012)

Zhao C, Gladstone R, Zwinger T, Gillet-Chaulet F, Wang Y, Caillet J, Mathiot P, Saraste L, Jager E, Galton-Fenzi BK, Christoffersen P and King MA (2025) Subglacial water amplifies Antarctic contributions to sea-level rise. *Nature Communications*, **16**(1), 3187 (doi: 10.1038/s41467-025-58375-4)

APPENDIX

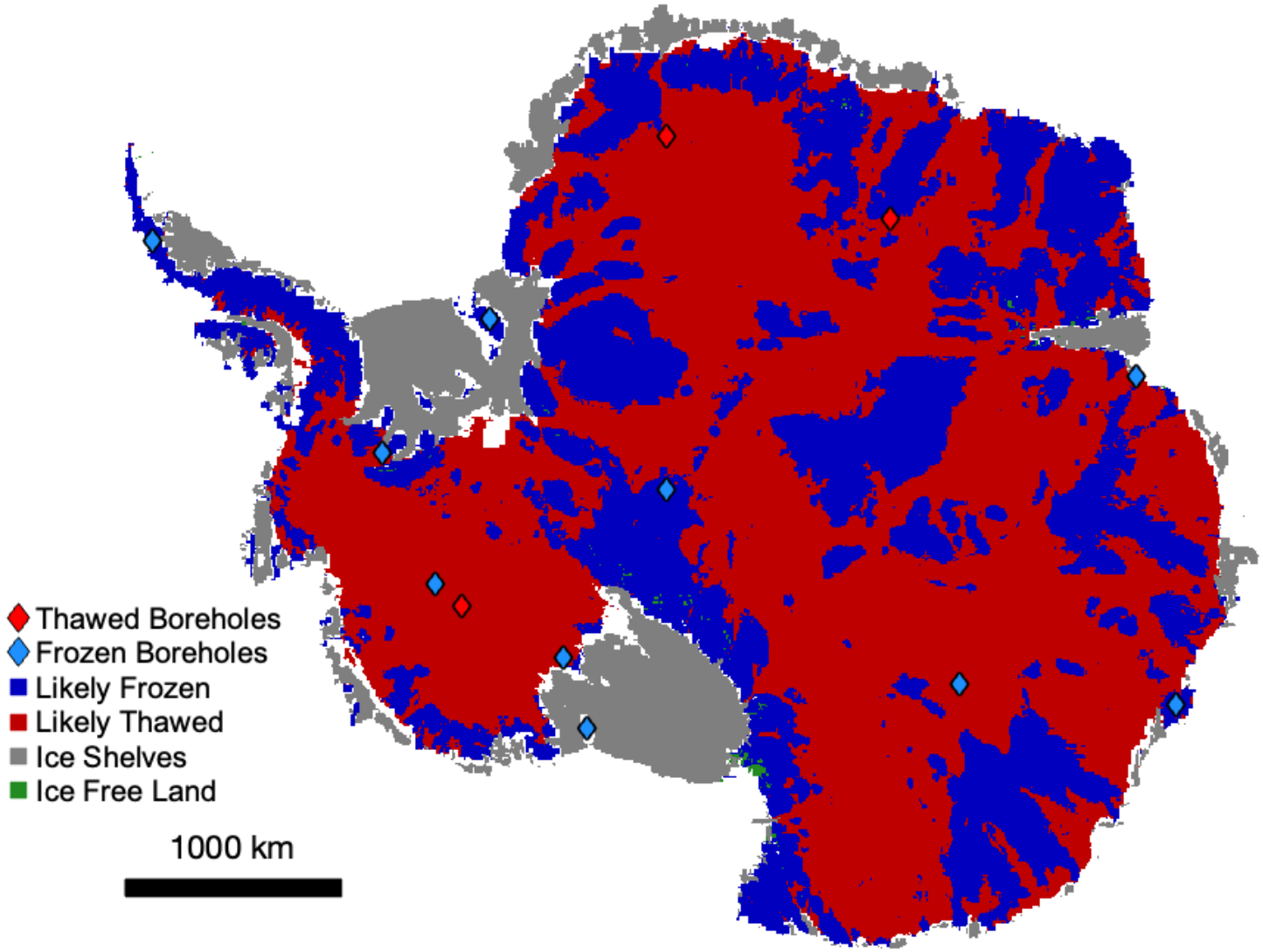

Fig. 9. Binary ISMIP6 agreement map, with regions in red where $\geqslant 5$ models predict temperatures above $-1°C$, and therefore a thawed bed, and blue where $\geqslant 5$ models predict temperatures below $-1°C$, and therefore a frozen bed. Red and blue diamonds indicate boreholes with thawed and frozen basal temperature, respectively.